# Crack Initiation in Functionally Graded Materials Under Mixed Mode Loading: Experiments and Simulations

**Alpay Oral**
Department of Mechanical Engineering,
Bogazici University,
34342 Bebek,
Istanbul, Turkey

**John Lambros**
Department of Aerospace Engineering,
University of Illinois, Urbana-Champaign,
Urbana, IL 61801

**Gunay Anlas**
Department of Mechanical Engineering,
Bogazici University,
34342 Bebek,
Istanbul, Turkey

*In this work, quasistatic crack initiation under mixed mode loading in planar (two-dimensional plane stress) functionally graded materials (FGMs) is studied. The goal of this work is to directly compare experiments and simulations so as to evaluate the applicability of the maximum tangential stress (MTS) criterion in predicting crack kinking in FGMs. Initially, crack initiation in the homogeneous material, which forms the basis of our FGM—polyethylene—is studied. The (generalized) maximum tangential stress is applied through the use of finite elements to determine crack initiation angles in the same graded configurations studied experimentally. Computational results of fracture parameters (stress intensity factors and T-stress), and crack initiation angles are compared to experimental results and good agreement is obtained. It is seen that the MTS criterion is applicable to FGM crack initiation prediction if the inherent material gradient length scale is larger than the fracture process zone.* [DOI: 10.1115/1.2936238]

*Keywords: FGM, crack initiation angle, mixed mode fracture, digital image correlation*

## 1 Introduction

As applied loading is seldom controlled in practice, it is common for a mixed mode stress field to develop in the vicinity of a notch or crack tip in a material. In general, this will involve all three modes of crack deformation: Modes I, II, and III, although the out-of-plane Mode III has received far less attention than the two in-plane Modes I and II. In homogeneous materials, crack growth is usually observed to occur under Mode I conditions, but crack initiation is dependent on the details of Modes I and II mix. Several criteria exist for predicting when a crack in a homogeneous material will initiate under mixed mode loading conditions. The two most common are the maximum tangential stress (MTS) criterion, $(\sigma_{\theta\theta})_{\max}$ [1], and the maximum strain energy release rate criterion, $G_{\max}$ [2]. Both have shown good agreement with experiments for quasibrittle homogeneous materials.

For the case of functionally graded materials (FGMs), the situation is further affected by the fact that near-tip mixity can arise by virtue of the property variation in the material even when far field loading is symmetric. Compared to homogeneous materials, mixed mode crack initiation in FGMs has received far less scrutiny. Most efforts are purely numerical and typically use finite element analyses (FEAs) to evaluate the validity of the above mentioned crack initiation criteria for FGMs. Becker et al. [3] found that, in contrast to homogeneous materials, for kink angles that maximize the energy release rate the Mode II stress intensity factor (SIF) $K_{\mathrm{II}}$ is not necessarily zero. This result was also confirmed experimentally in the work of Abanto-Bueno and Lambros [4]. Kim and Paulino [5], using a generalized MTS criterion that also includes the $T$-stress, found that positive $T$-stress values increase the crack initiation angle, and vice versa, when compared to the homogeneous case. In addition, they observed a significant influence of the FGMs' intrinsic degree of nonhomogeneity on the magnitude and sign of the $T$-stress.

Experimental studies on the mixed mode quasistatic loading of FGMs are very limited in number. Rousseau and Tippur [6] investigated the fracture behavior of FGMs with cracks perpendicular to the elastic gradient and found that the crack kinked toward the more compliant region, and both the MTS and the vanishing $K_{\mathrm{II}}$ criteria [7] could also be applied to predict the kinking angle in their FGMs. More recently, Abanto-Bueno and Lambros [4] performed an investigation of crack initiation and growth in FGMs that possessed near-tip mixity generated by either applied loading or material gradient, or both factors combined. They also found that for their FGMs the MTS criterion predicted kink angles well, although continued crack growth under mixed mode was possible with nonzero $K_{\mathrm{II}}$.

To date, however, there has been no attempt to combine the existing experimental and numerical studies in order to evaluate the validity of possible fracture criteria for more general situations. This is the goal of the present work. Our approach is to combine the experimental results of Abanto-Bueno and Lambros [4] with detailed numerical simulations of the precise material geometry and loading used in the experiments. In this fashion, a direct comparison between numerics and experiments can be made, thus providing a much better understanding of mixed mode crack initiation in FGMs.

## 2 Experiments

The experimental results used in this study are taken from those obtained by Abanto-Bueno and Lambros [4]. Details of the experimental methodology are described in that work and will not be repeated in the interest of brevity. Only the results relevant to the current work will be described here. The testing protocol of Abanto-Bueno and Lambros [4] included mixed mode fracture experiments on the base homogeneous material, polyethylene, used for manufacturing the FGMs. Subsequently, mixed mode fracture experiments were conducted on FGMs with near-tip mixity generated through either applied load/geometry asymmetry, or a material property gradient inclined to the crack tip, or both.

The graded FGM samples were manufactured using selective ultraviolet (UV) light irradiation on a photodegradable polyethylene carbon monoxide copolymer. Typically, a thin sheet (thickness

Contributed by the Applied Mechanics Division of ASME for publication in the JOURNAL OF APPLIED MECHANICS. Manuscript received June 29, 2007; final manuscript received December 31, 2007; published online July 11, 2008. Review conducted by Marek-Jerzy Pindera.

  

of 0.406 mm) of in-plane dimensions $300\times150$ mm$^2$ was irradiated for times varying from 5 h to 300 h. After irradiation, the sheet was cut in half parallel to the irradiation direction, and two samples of $150\times150$ mm$^2$ were obtained. One of these was then cut perpendicularly to the irradiation direction into 15 strips of 10 mm width, which were used in uniaxial tension tests to measure elastic and failure property variation as a function of position on the sample. The remaining $150\times150$ mm$^2$ sample from the original sheet was then used for a single edge notch fracture experiment. Therefore, the variation of local material properties such as elastic modulus, failure stress, and failure strain was measured independently of the fracture experiments, but originating from exactly the same manufacturing process. By measuring local properties in this fashion for every experiment material, variability issues were circumvented.

Figure 1 shows the elastic modulus variation for three FGM cases: Case I, Fig. 1(*a*), which possesses a symmetric geometry, but the material property gradient is perpendicular to the crack line; Case II, Fig. 1(*b*), in which mixity is introduced by an asymmetry in both geometry and material property gradient; and Case III, Fig. 1(*c*), in which the material property gradient is parallel to the crack line, but the loading is not.

Fracture experiments were conducted in which detailed near-tip full-field experimental data were obtained throughout crack initiation and growth. In the present work, we will only concentrate on the crack initiation results and compare them to companion numerical simulations. Both components of the in-plane crack tip displacement field were measured experimentally using the digital image correlation (DIC) technique [8]. The theoretical asymptotic near-tip opening displacement field, denoted here as $u_y$, for a homogeneous isotropic linearly elastic material subjected to in-plane mixed mode loading is given by

$$u_y = \frac{K_I}{2\mu}\left(\frac{r}{2\pi}\right)^{1/2}\sin\frac{\theta}{2}\left(\frac{3-\nu}{1+\nu}-\cos\theta\right)-\frac{T\nu}{2\mu(1+\nu)}r\sin\theta + \frac{K_{II}}{4\mu}\left(\frac{r}{2\pi}\right)^{1/2}\left(\frac{5\nu-3}{1+\nu}\cos\frac{\theta}{2}-\cos\frac{3\theta}{2}\right)+A_1 r\cos\theta+u_{0y} \tag{1}$$

where $A_1$ and $u_{0y}$ represent rigid body rotation and translation, respectively, $\nu$ is Poisson's ratio and $\mu$ is the shear modulus of the material, and $r$ and $\theta$ are polar coordinates centered at the crack tip. Three terms associated with the crack tip field itself are shown in Eq. (1)—those corresponding to the mixed mode SIFs $K_I$ and $K_{II}$, and the $T$-stress. The $T$-stress term represents a stress component parallel to the crack line and is highly dependent on specimen configuration and loading. For the case of a FGM, the properties used in Eq. (1) are those measured at the crack tip, and are denoted as $\nu_{tip}$ and $\mu_{tip}$.

All three values of $K_I$, $K_{II}$, and $T$, as well as the constants for rigid body motion $A_1$ and $u_{0y}$, are obtained simultaneously by performing a least squares fit of experimental DIC values to Eq. (1). It is important to note that in purely $K$-dominant field the $T$-stress term in Eq. (1) would be negligible. Abanto-Bueno and Lambros [4] found that for the configurations used here, the $K$-dominant field often times did not represent the experimentally measured displacement fields well, and the $T$-stress had to be included to get a good comparison. The importance of $T$-stress in this configuration can be judged by the experimental results shown in Tables 1 and 3. Depending on the specimen geometry and gradient, the $T$-stress ranged from −0.069 MPa to over −4.2 MPa. The importance of the $T$-stress should be judged not only with respect to the singular term (i.e., amount of stress biaxiality), but also with respect to the yield stress of the material. The biaxiality ratio, defined here for a mixed mode situation as $\beta=T\sqrt{(\pi a)}/\sqrt{(K_I^2+K_{II}^2)}$, is a relative measure of $T$-stress compared to the singular field. Values of experimentally obtained biaxiality for each case are shown in Tables 1 and 3. In addition, for

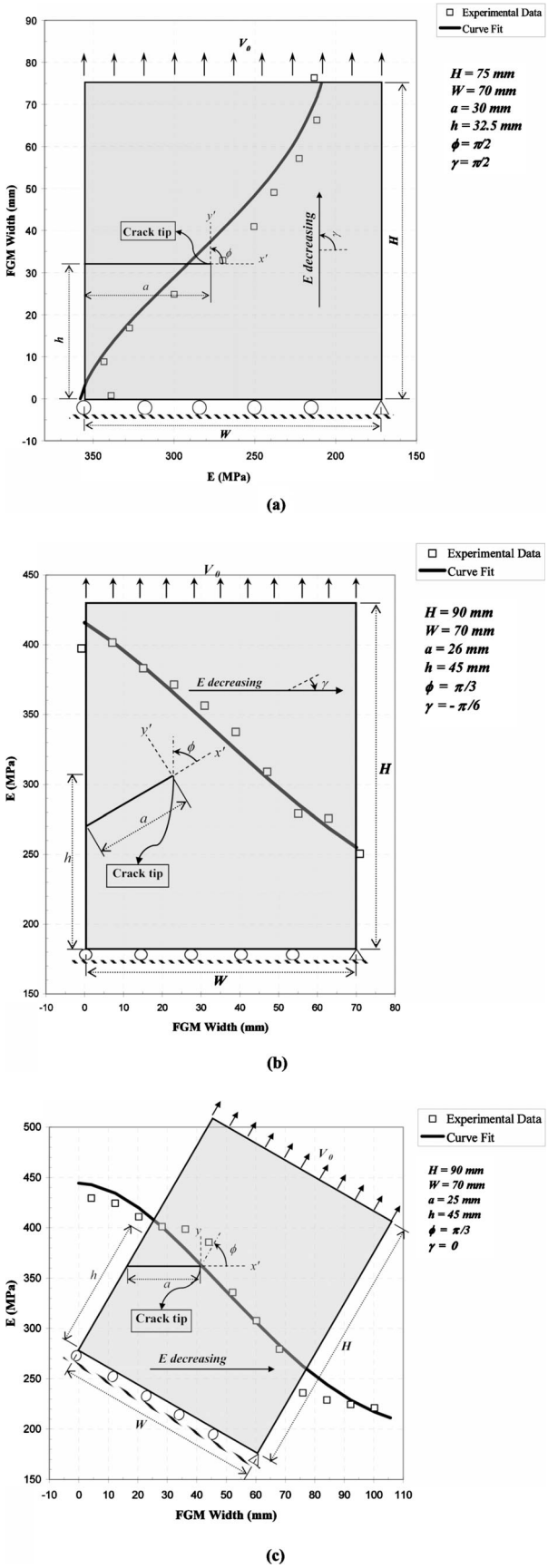


**Fig. 1 Geometry, loading, and elastic modulus variation for three FGM specimens used in Ref. [4]: (*a*) Case I, symmetric loading and nonsymmetric property gradient; (*b*) Case II, nonsymmetric loading and property gradient; and (*c*) Case III, symmetric gradient and nonsymmetric loading**

**Table 1 Experimental and numerical results for $K_I$, $K_{II}$, and $T$-stress, for homogeneous edge cracked specimen**

| | $K_I$ (MPa m$^{0.5}$) | $K_{II}$ (MPa m$^{0.5}$) | $T$ (MPa) | Biaxiality $\beta$ |
|---|---|---|---|---|
| Expt. results | 0.903 | 0.245 | −0.784 | −0.270 |
| Num. results | 0.793 | 0.212 | −0.992 | |

the polyethylene used here, the yield stress varies between 8 MPa and 12 MPa [4]. Therefore, a value of −4.272 MPa $T$-stress is very significant, whereas a value of −0.069 MPa corresponds to an almost $K$-dominant situation. Thus, the presence of $T$-stress can significantly affect the values of $K_I$ and $K_{II}$ in many cases, and has therefore been included in Eq. (1).

Figure 2 shows the final cracked geometry in each of the three FGM cases after loading. Crack kinking is evident in each case. However, the crack initiation angle was measured after each experiment using an optical microscope to zoom into the crack tip.

## 3 Numerical Simulations

Finite element simulations were conducted using MSC.Marc® 2005r3 [9]. An example of a mesh used in the simulations is shown in Fig. 3(*a*). The entire plate used in the fracture experiments in Ref. [4] is discretized with between 3300 and 3600 four node quadratic plane stress elements. Since for each specimen, whether homogeneous or FGM, the dimensions and geometry tested in Ref. [4] are somewhat different, each case was discretized separately. Note, therefore, that in some cases the crack would be horizontal, unlike what is shown in Fig. 3(*a*). However, to allow for comparison between all cases, the near-tip discretization was kept the same, and consisted of a focused mesh centered at the crack tip out to a radius of $r/a=0.2$, where $r$ is the radial coordinate (defined in Fig. 3(*c*)) and $a$ is the crack length for each specimen. The focused portion of the mesh consisted of 36 elements along the tangential direction, and 14 elements along the radial direction, with a total of 504 elements as shown in Fig. 3(*b*). The remainder of each specimen outside of this region was automeshed by the software package used, thus accounting for the irregular mesh shape outside the focused region, and for the dif-

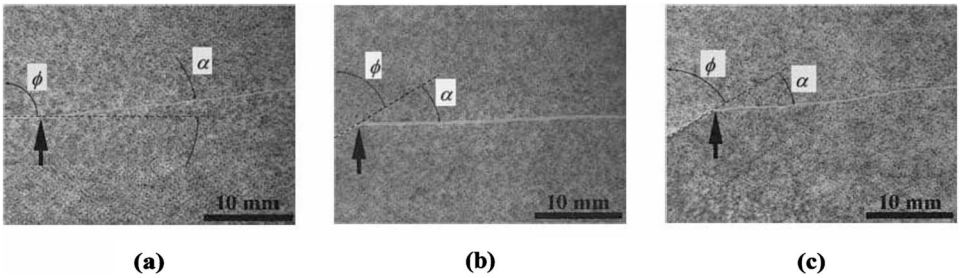


**Fig. 2 Photograph of the final crack path for (*a*) Case I, (*b*) Case II, and (*c*) Case III from the experiments of Abanto-Bueno and Lambros [4]**

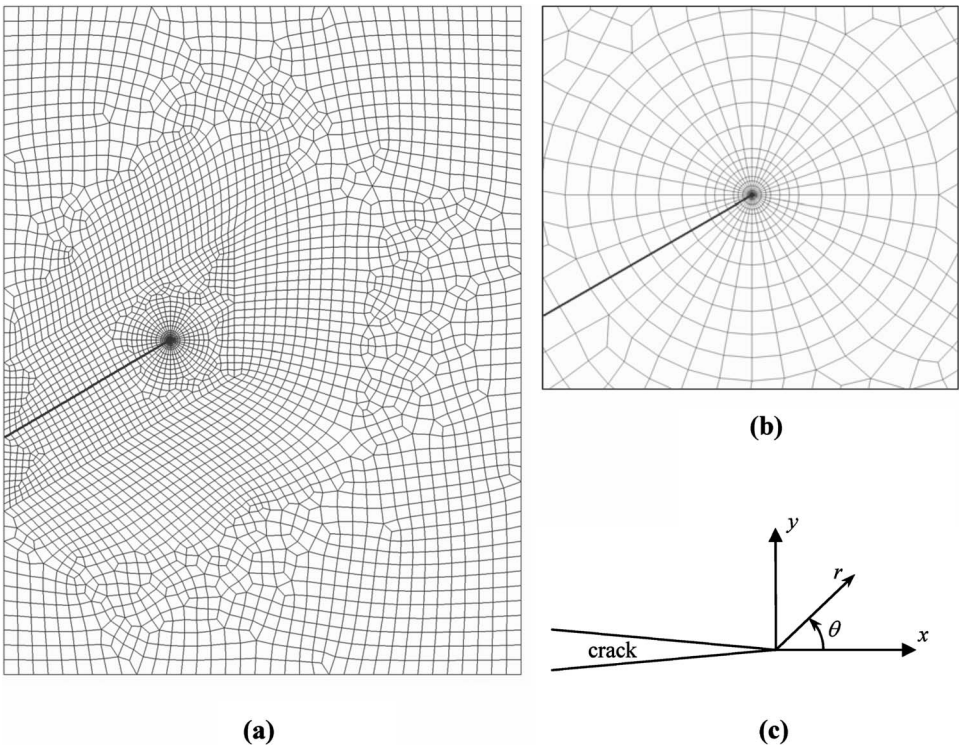


**Fig. 3 Typical finite element mesh used for (*a*) complete model and (*b*) near crack tip. (*c*) Shows the local coordinate system at the crack tip. All quantities must be rotated into this coordinate system.**

**Table 2 Experimental and numerical results for crack initiation angle for homogeneous edge cracked specimen**

| Crack initiation angles, $\alpha$ (deg) | | | | | |
|---|---|---|---|---|---|
| Expt. | FE—Using $(\sigma_{\theta\theta})_{max}$ | | Using GMTS, Eq. (4) | | Using MTS, Eq. (4), $r_c=0$ |
| $-28\pm1.5$ | $-31.5$ | for $r/a=0.01$ | $-24.1$ | for $r_c/a=0.01$ | $-26.7$ |
| | $-30.8$ | for $r/a=0.02$ | $-23.1$ | for $r_c/a=0.02$ | |
| | $-30.1$ | for $r/a=0.05$ | $-21.3$ | for $r_c/a=0.05$ | |
| | $-29.7$ | for $r/a=0.1$ | $-19.6$ | for $r_c/a=0.1$ | |

ference in the total number of elements in each case.

The specimen dimensions used in each case were those reported in Ref. [4]. The specimen thickness, common to all homogeneous and FGM samples, was 0.406 mm. Loading was applied as a fixed vertical displacement boundary condition along the upper edge of the specimen because the experiments of Abanto-Bueno and Lambros [4] were conducted under displacement control. Since the focus of this work is to study mixed mode crack initiation, and assuming a quasistatic loading process, the value of the displacement applied in the simulations was exactly that recorded in each experiment *at the precise instant of crack initiation*. In addition to the applied displacement along the upper edge, the vertical displacement was set to 0 at the lower edge, matching the experimental setup, and the horizontal displacement was set to 0 at the lower right hand corner in order to eliminate rigid body motion (Fig. 3(*a*)). Material properties used were also those measured experimentally. More details on the allocation of material properties in the FGM case are given below. In both the homogeneous and graded cases, the material was assumed to behave in a linear elastic fashion. The material used in Ref. [4] was UV light irradiated polyethylene, which after irradiation failed by crazing while showing very little shear yielding. The linear elastic assumption therefore should be applicable, and was, in fact, also made in the data analysis of Abanto-Bueno and Lambros [4].

Abanto-Bueno and Lambros [4] used the full-field method of DIC to measure the displacement field in an area surrounding the crack tip. They then extracted fracture quantities $K_I$, $K_{II}$, and $T$ as described in the previous section. In the present work, the simulations provide full-field stress and displacement fields, which must then be processed to provide $K_I$, $K_{II}$, and $T$. $K_I$ and $K_{II}$ can reasonably be obtained from FEA; but, there are few reliable methods of obtaining $T$-stress from the full-field stress field. One methodology involving the difference of $\sigma_{xx}-\sigma_{yy}$ near the crack tip is presented in Ref. [10]. This method was attempted, but yielded unclear results usually producing a large variation of the constant $T$-stress around the crack tip. A more robust method using an interaction integral approach is presented in Ref. [5]. However, this technique is computationally more involved and was not available for FGMs in the software package used. Therefore, since the FEA simulations produce full-field displacement data similar to the DIC experiments, it was decided to use the same procedure as in the experiments, i.e., the least squares fitting of $u_y$ in Eq. (1) to the full-field displacement, to extract values of $K_I$, $K_{II}$, and $T$. These values are somewhat sensitive to the area around the crack tip selected for the fitting process, but through an iterative scheme it is possible to obtain convergent values of the three quantities that fit the displacement field around the crack tip extremely well. More details about this issue are given in Sec. 5.

## 4 Results

**4.1 Homogeneous Material.** The base homogeneous material studied is a 0.406 mm thick polyethylene cocarbon monoxide sheet irradiated for 50 h under UV light. Its elastic properties were measured in Ref. [4] as Young's modulus $E=280$ MPa and Poisson's ratio $\nu=0.45$. Mixed mode loading in the homogeneous case was generated by inclining the crack in an otherwise symmetrically loaded single edge cracked plate, as shown in Fig. 4.

Using the procedure outlined in the previous section, values of $K_I$, $K_{II}$, and $T$ were extracted from the finite element simulations corresponding to the experimentally recorded instant of crack initiation. Table 1 shows a comparison of these values with the corresponding experimental results given in Ref. [4]. The results agree reasonably well, especially for quantities $K_{II}$ and $T$, which are usually more difficult to obtain.

The MTS criterion states that a crack will grow perpendicular to the direction of MTS, $\sigma_{\theta\theta}$ [1,11]. The FEA results provide as an output $\sigma_{\theta\theta}$, whose maximum for a given $r$ is easy to establish. The stress results are rotated into a coordinate frame shown in Fig. 3(*c*), and the angle at which the maximum $\sigma_{\theta\theta}$ occurs is recorded. This can vary as a function of $r$, as shown in Table 2. The comparison with the experimentally measured kink angle value of $-28$ deg $\pm$ 1.5 deg is good especially for $r/a=0.1$.

The MTS criterion can also be cast in terms of SIFS by computing the angle for which $\sigma_{\theta\theta}$ predicted by the asymptotic field is maximum. Using only the singular term in the asymptotic expansion for stresses produces a unique kink angle independent of $r$. However, in the configuration used in the experiments of Abanto-Bueno and Lambros [4], large values of $T$-stress were measured compared to $K_I$ and $K_{II}$ (e.g., Table 1). Therefore, the effect of $T$-stress may need to be taken into account in determining the crack kinking angle using the so-called generalized maximum tangential stress (GMTS) criterion [11]. The asymptotic equation for $\sigma_{\theta\theta}$ to second order is [11]

$$\sigma_{\theta\theta}=\frac{1}{\sqrt{2\pi r}}\cos\frac{\theta}{2}\left[K_I\cos^2\frac{\theta}{2}-\frac{3}{2}K_{II}\sin\theta\right]+T\sin^2\theta \quad (2)$$

Using the GMTS criterion, the crack initiation angle $\alpha$ can then be obtained along the direction of MTS, from

$$\frac{\partial\sigma_{\theta\theta}}{\partial\theta}=0\Rightarrow\theta=\alpha \quad (3)$$

Substituting Eq. (2) into Eq. (3) yields

$$K_I\sin\alpha+K_{II}(3\cos\alpha-1)-\frac{16}{3}T\sqrt{2\pi r_c}\sin\frac{\alpha}{2}\cos\alpha=0 \quad (4)$$

where $r_c$ is a length scale, considered a material property, at which the tangential stress must reach a critical value. If $r_c$ is 0, Eq. (4) reduces to the MTS criterion result. Since $r_c$ is external to the theory, it can only be obtained by comparison with experiments. This is usually done by conducting experiments over a range of mode mixity and finding a single value of $r_c$ with which the predictions of Eq. (4) agree with experiments in Ref. [12]. Unfortunately, in the present work, we have experimental results for a single mode mixity; therefore, we cannot directly determine a value for $r_c$.[1] Therefore, in Table 2, we present the predictions of the MTS criterion along with the GMTS theory using the values

[1]Note that although it is feasible to obtain different mode mixities for the homogeneous case, it is virtually impossible for the FGM case, which would require testing of FGMs with exactly the same material property variation, but different loading conditions.

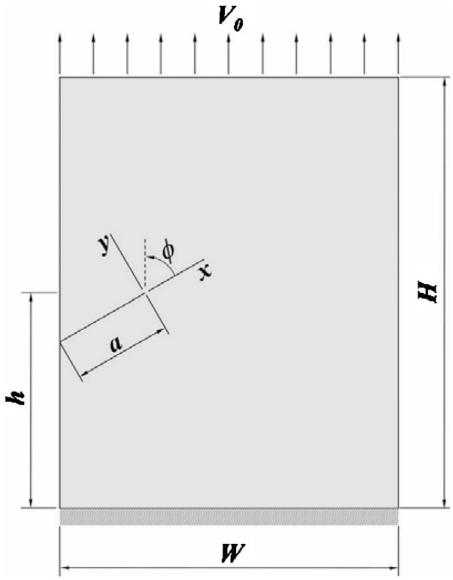


**Fig. 4 Edge cracked specimen geometry for homogeneous material ($V_0$ is the applied displacement), $H$=90 mm, $W$ =70 mm, $h$=45 mm, $a$=33 mm, and $\phi=\pi/3$**

of $K_I$, $K_{II}$, and $T$ obtained in the FEA (Table 1) and various values of $r_c$. The results are again in good agreement with the experiments, with the MTS result being closest to the experimental one.

**4.2 Graded Material.** The loading geometry and elastic modulus distribution for the three FGM cases are shown in Fig. 1. In all three cases, Poisson's ratio $\nu$ was taken as constant at 0.45. The three FGMs have been designed such that the local mode mixity is generated by a host of different methods. In Case I, mode mixity is a result solely of material gradient orientation. In Case II, it is a result of both loading and material gradient asymmetry. Finally, in Case III, the crack is parallel to the material gradient and asymmetry is introduced only from a loading asymmetry.

The finite element simulation procedure for the FGM specimens is similar to that used for the homogeneous material. The loading applied in the simulations is again the displacement measured at crack initiation. The main difference is the allocation of varying elastic properties to the discretization shown in Fig. 1. One option is to assign material properties at Gauss quadrature points in each element [13,14]. A second option, employed in the present work, is to provide an elastic modulus variation by assuming temperature dependent modulus and providing the material with an initial temperature distribution to match the elastic modulus variation desired.

Results for the fracture parameters $K_I$, $K_{II}$, and $T$-stress, presented in Table 3, are obtained following the procedure used for the homogenous case, with the exception of $\mu_{tip}$ and $\nu_{tip}$ used in the least squares fitting process of Eq. (1). Crack initiation angles are also obtained by identifying the radial direction along which the tangential stress $\sigma_{\theta\theta}$ is maximum. Figure 5 shows the variation

**Table 3 Experimental and numerical results for $K_I$, $K_{II}$, and $T$-stress for the FGM edge cracked specimens**

| | Case | $K_I$ (MPa m$^{0.5}$) | $K_{II}$ (MPa m$^{0.5}$) | $T$ (MPa) | Biaxiality $\beta$ |
|---|---|---|---|---|---|
| Expt. results | I | 0.554 | 0.039 | −4.272 | −2.361 |
| Num. results | | 0.551 | −0.022 | −2.149 | |
| Expt. results | II | 0.755 | 0.179 | −0.069 | −0.025 |
| Num. results | | 0.722 | 0.204 | −0.673 | |
| Expt. results | III | 0.969 | 0.224 | −0.930 | −0.262 |
| Num. results | | 0.878 | 0.230 | −0.870 | |

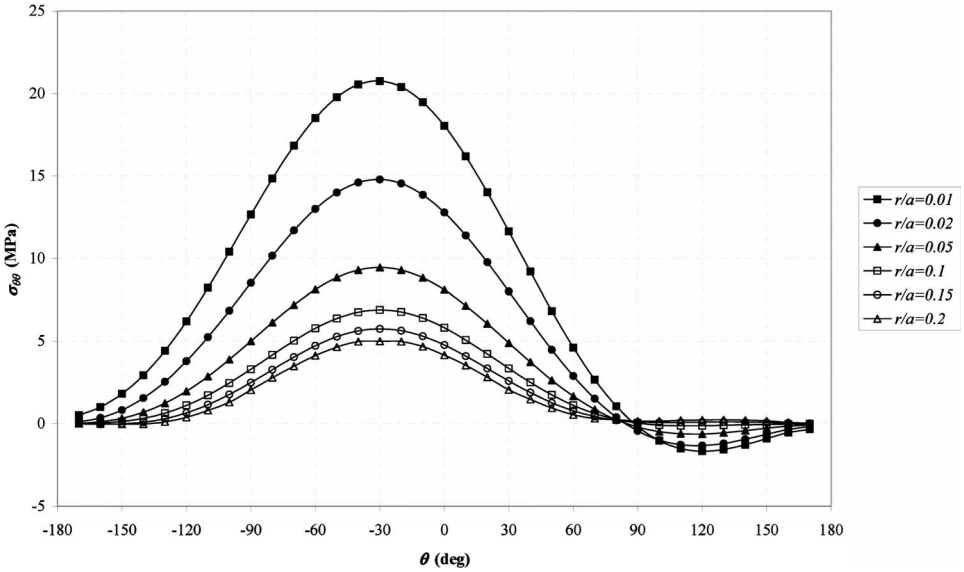


**Fig. 5 Variation of $\sigma_{\theta\theta}$ with angle around the crack tip for specific radial directions obtained numerically for the FGM in Case II**

**Table 4 Experimental and numerical results for crack initiation angles for the FGM edge cracked specimens**

| | Crack initiation angles, $\alpha$ (deg) | | | | |
|---|---|---|---|---|---|
| | Expt. | FE—using $(\sigma_{\theta\theta})_{max}$ | | Using GMTS, Eq. (4) | Using MTS, Eq. (4), $r_c=0$ |
| Case I | $0 \pm 1.5$ | 2.3 | for $r/a=0.01$ | 3.1 for $r_c/a=0.01$ | 4.6 |
| | | 2.0 | for $r/a=0.02$ | 2.8 for $r_c/a=0.02$ | |
| | | 1.2 | for $r/a=0.05$ | 2.3 for $r_c/a=0.05$ | |
| | | 0.5 | for $r/a=0.1$ | 1.9 for $r_c/a=0.1$ | |
| Case II | $-28 \pm 1.5$ | −31.3 | for $r/a=0.01$ | −26.0 for $r_c/a=0.01$ | −27.8 |
| | | −30.7 | for $r/a=0.02$ | −25.3 for $r_c/a=0.02$ | |
| | | −30.1 | for $r/a=0.05$ | −24.0 for $r_c/a=0.05$ | |
| | | −29.8 | for $r/a=0.1$ | −22.6 for $r_c/a=0.1$ | |
| Case III | $-19 \pm 1.5$ (Crack growth size smaller than initial craze) | −30.2 | for $r/a=0.01$ | −24.4 for $r_c/a=0.01$ | −26.3 |
| | | −29.7 | for $r/a=0.02$ | −23.7 for $r_c/a=0.02$ | |
| | | −29.3 | for $r/a=0.05$ | −22.4 for $r_c/a=0.05$ | |
| | $-26 \pm 1.5$ (Crack growth size larger than initial craze) | −29.3 | for $r/a=0.1$ | −21.0 for $r_c/a=0.1$ | |

of tangential stress with angle around the tip for different radial distances for the FGM of Case II. For the discretization used here, the maximum is clearly identifiable. As in the homogeneous case, there is a small radial dependence of the location of maximum $\sigma_{\theta\theta}$ away from the tip, likely a result of the relatively large $T$-stress present in this configuration. The experimentally measured and numerically predicted crack initiation angles are given in Table 4, along with the predictions of the MTS and GMTS models.

## 5 Discussion

In Tables 1 and 3, $K_I$, $K_{II}$, and $T$-stresses are computed from both the numerical and experimental results using a least squares fit to Eq. (1). In general, $K_I$, $K_{II}$, and $T$-stresses are in reasonably good agreement between experiments and numerical analysis, although there are some important deviations. As discussed earlier, $T$-stress is a difficult quantity to extract both numerically and experimentally. Therefore, the largest discrepancies appear there. The configurations used in the experimental study produce a large $T$-stress variation, which is also affected by the property gradient direction. The experimental values of $T$-stress obtained at crack initiation range from −4.272 MPa to −0.069 MPa depending on geometry and gradient, but are always negative.

All the results, especially the $T$-stress, are affected by the region where the least squares minimization is applied. Experimentally measured displacements are fitted to the asymptotic displacement equation by excluding a rectangular region around the crack tip where the digital image correlation cannot be performed. In the numerical case, however, data as close to the crack tip as is desired can be included in the fit—especially given the fact that the simulations are purely elastic whereas in the experiments failure occurs by crazing. We conducted a series of least square fits to the FEA data including points increasingly closer to the crack tip. The results in Table 3 are obtained when using the FEA displacement field down to the fifth ring of elements around the tip ($r/a=0.02$). A negative value of $K_{II}$ is obtained in Case I, in contrast to the positive value measured experimentally. The value of $K_{II}$ is relatively small in Case I, but the sign affects the direction of crack kinking. Although at initiation in the experiment the crack appears to grow straight, it does kink in a positive direction of about 7 deg ± 1.5 deg after about 2 mm of crack growth (see Fig. 2(*a*)). The *positive* value of $K_{II}$ obtained experimentally incorrectly predicts a small *negative* kink angle [4]. The numerical results obtained here, when fitted to displacement data very near the crack tip, provide a *negative* $K_{II}$, which correctly predicts the *positive* sign of subsequent crack kinking. Care must therefore be taken in extracting fracture parameters solely from experiments, especially regarding the sign of $K_{II}$ when it is small.

The GMTS criterion was used either directly form the FEA or through use of the asymptotic equation (4) to predict crack initiation angle, $\alpha$. Except for Case III, predicted crack initiation angles are generally in good agreement with the experimentally measured ones. In Case III, −19 deg is quoted in Ref. [4] for kink angle. However, this value was obtained right after crack kinking, for extremely small crack kink length, as seen in Fig. 6. Although strictly speaking this is the appropriate scale to determine the kink angle, the crack extension in Fig. 6 is comparable to the craze length, and therefore is clearly not elastic. The details of the stress field associated with the mixed mode craze dominate the crack deflection in Fig. 6. It is therefore unreasonable to expect a good comparison with a purely elastic simulation. If one allows the crack to grow to a size much larger than the initial craze, as seen in Fig. 2(*c*), an angle of −26 deg is found for the kinking angle, which compares much better with elastic FEA results. This discrepancy between near- and far-field kink angles is not as prevalent in Cases I and II because in Case I the angles involved (and the value of $K_{II}$) are small, and in Case II right after the crack

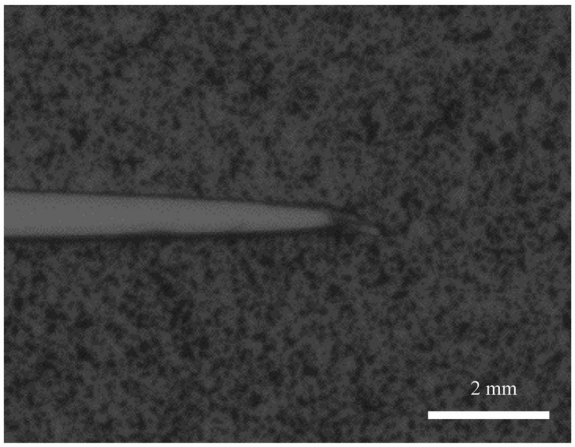


**Fig. 6 Close-up photograph showing initial crack kinking for Case III FGM**

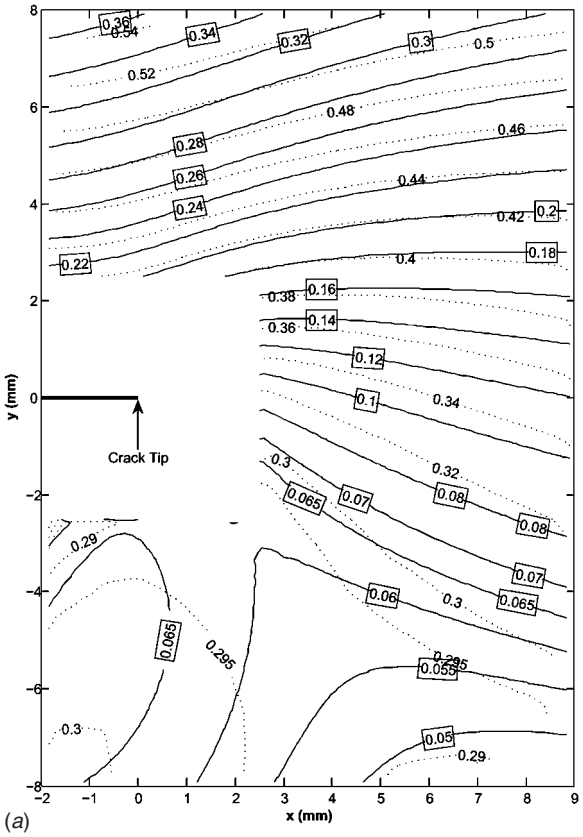


(*a*)

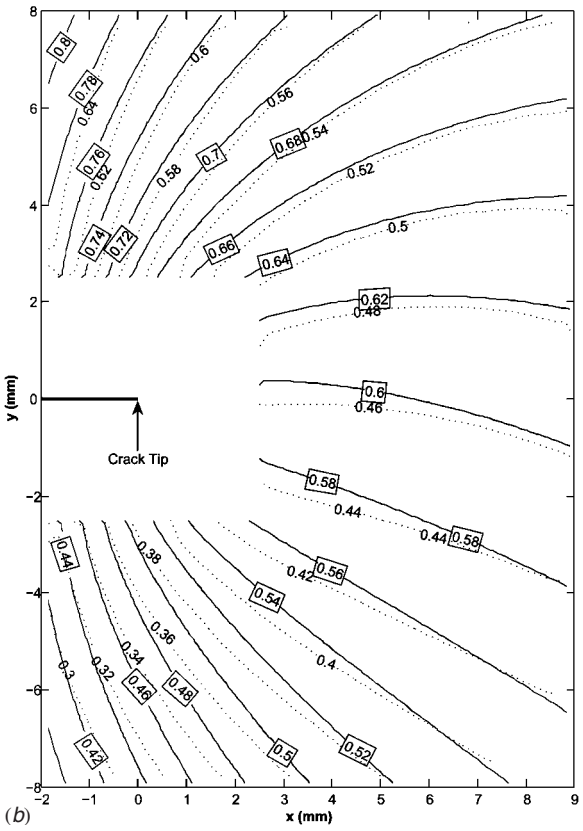


(*b*)

**Fig. 7 Contours of (*a*) $u_x$ and (*b*) $u_y$ for Case III (solid lines and values in boxes are experimental results, and dashed lines, and values without boxes are numerical results)**

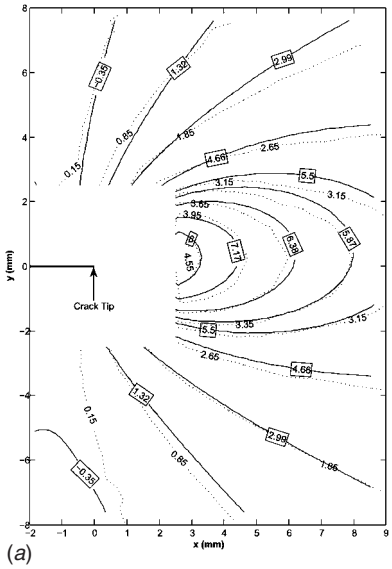


(*a*)

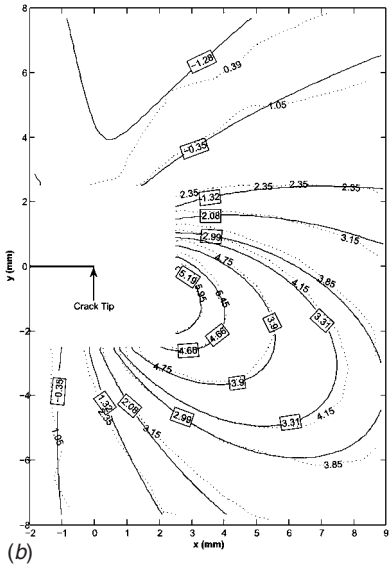


(*b*)

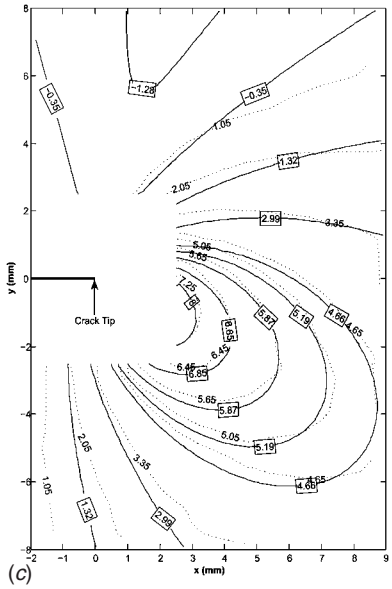


(*c*)

**Fig. 8 Contours of $\sigma_{\theta\theta}$ for (*a*) Case I, (*b*) Case II, and (*c*) Case III (solid lines and values in boxes are experimental results, and dashed lines and values without boxes are numerical results)**

kinks it becomes Mode I, by virtue of the geometry and material gradient. However, in Case III, continued mode mixity is seen at the crack tip as the crack grows.

The full-field nature of both the DIC experimental measurements and the FEA numerical results also allow for a comparison of displacement and stress fields around the crack tip. The two in-plane displacement components are the fundamental measurement made by DIC. Figure 7 shows contour plots comparing the experimentally measured and numerically predicted displacement field at the time of crack initiation for Case III. Although the values are somewhat different, especially for $u_x$, the fields are very similar. In the work of Abanto-Bueno and Lambros [4], stresses were also derived by using the DIC displacement measurements to calculate strain and then, knowing the local material properties, calculate stress by taking into account the material nonhomogeneity. Figure 8 shows a comparison of $\sigma_{\theta\theta}$ contours obtained numerically and experimentally for Cases I–III. The values of stress at the same contour level for Cases I and II differ substantially. Agreement is far better for Case III. The discrepancy is likely a result of the fact that stresses are not directly measured by DIC, but have to be calculated through a multistep process involving differentiation and interpolation by combining the displacement data and local material properties. As such, the stresses are particularly susceptible to property discretization errors, both on the FEA side and on the experimental side. However, the good agreement in Case III is encouraging. In addition, the shape of the contour lines in all three cases is very similar. As a result, the MTS direction, which predicts the crack initiation angle, is the same for each case.

## 6 Conclusions

Quasistatic crack initiation in FGMs subjected to mixed mode loading was studied in this work. The goal of the study was to directly compare as closely as possible experiments and simulations in order to evaluate the applicability of the GMTS criterion in predicting crack kinking in FGMs. The MTS criterion was seen to predict the kinking response in homogeneous polyethylene well. For the FGM case, fracture parameters of SIFs and $T$-stress were compared to experimental results and good agreement was obtained. However, it was found that to correctly predict the sign of $K_{II}$ care needs to be taken in the process in which $K_{II}$ is extracted when a least squares fitting approach is employed. This has significant implications for many optical experimental techniques used in fracture mechanics, which limit the amount of data accessible in the crack tip region. Using the GMTS criterion, either directly from the finite elements or from the fracture parameters extracted from FEA, provided reasonably good values for the experimentally measured kink angles for crack extensions larger than the craze length. Therefore, we can conclude that the MTS criterion is applicable to FGM crack initiation prediction if the inherent material gradient length scale is larger than the fracture process zone.

## Acknowledgment

This study was supported by the National Science Foundation (NSF) through Grant No. NSF-INT-0322271. G.A. and A.O. acknowledge partial support of the State Planning Agency (DPT) through Grant No. DPT 01 K 120270.

## References

[1] Erdogan, F., and Sih, G. C., 1963, "On the Crack Extension in Plates Under Plane Loading and Transverse Shear," ASME J. Basic Eng., **85**(4), pp. 519–525.
[2] Cotterell, B., 1965, "On the Brittle Fracture Paths," Int. J. Fract. Mech., **1**(2), pp. 96–103.
[3] Becker, T. L., Cannon, R. M., and Ritchie, R. O., 2001, "Finite Crack Kinking and T-Stresses in Functionally Graded Materials," Int. J. Solids Struct., **38**,(32–33), pp. 5545–5563.
[4] Abanto-Bueno, J., and Lambros, J., 2006, "An Experimental Study of Mixed Mode Crack Initiation and Growth in Functionally Graded Materials," Exp. Mech., **46**(2), pp. 179–196.
[5] Kim, J.-H., and Paulino, G. H., 2003, "T-Stress, Mixed-Mode Stress Intensity Factors, and Crack Initiation Angles in Functionally Graded Materials: A Unified Approach Using the Interaction Integral Method," Comput. Methods Appl. Mech. Eng., **112**(11–12), pp. 1463–1494.
[6] Rousseau, C.-E., and Tippur, H. V., 2000, "Compositionally Graded Materials With Cracks Normal to the Elastic Gradient," Acta Mater., **48**(16), pp. 4021–4033.
[7] He, M.-Y., and Hutchinson, J. W., 1989, "Kinking of a Crack Out of an Interface," ASME J. Appl. Mech., **56**, pp. 270–278.
[8] Peters, W. H., and Ranson, W. F., 1982, "Digital Imaging Techniques in Experimental Stress Analysis," Opt. Eng. (Bellingham), **21**(3), pp. 427–431.
[9] MSC.MARC®, User Documentation, version 2005r3, MSC.Software Corporation, 2 MacArthur Place, Santa Ana, CA 92707.
[10] Ayatollahi, M. R., Pavier, M. J., and Smith, D. J., 1998, "Determination of $T$-Stress From Finite Element Analysis for Mode I and Mixed Mode I/II Loading," Int. J. Fract., **91**(3), pp. 283–298.
[11] Williams, J. G., and Ewing, P. D., 1972, "Fracture Under Complex Stress—Angled Crack Problem," Int. J. Fract., **8**(4), pp. 441–446.
[12] Chen, C. S., Wawrzynek, P. A., and Ingraffea, A. R., 1999, "Crack Growth Simulation and Residual Strength Prediction in Airplane Fuselages," NASA/CR-1999-209115.
[13] Santare, M. H., and Lambros, J., 2000, "Use of Graded Finite Elements to Model the Behavior of Nonhomogeneous Materials," ASME J. Appl. Mech., **67**(4), pp. 819–822.
[14] Kim, J.-H., and Paulino, G. H., 2002, "Isoparametric Graded Finite Elements for Nonhomogeneous Isotropic and Orthotropic Materials," ASME J. Appl. Mech., **69**(4), pp. 502–514.